Journal of Molecular Structure 1259 (2022) 132764

Contents lists available at ScienceDirect

Journal of Molecular Structure

journal homepage: www.elsevier.com/locate/molstr

Texture and morphology-directed activity of magnesia-silica mixed oxide catalysts of ethanol-to-butadiene reaction

Blanka Szabó[a], Gyula Novodárszki[a], Ferenc Lónyi[a], László Trif[a], Zsolt Fogarassy[b], József Valyon[a], Róbert Barthos[a,*]

[a] Institute of Materials and Environmental Chemistry, Research Centre for Natural Sciences, Magyar tudósok körútja 2, Budapest 1117, Hungary
[b] Centre for Energy Research, Institute for Technical Physics and Materials Science, Konkoly-Thege M. út 29-33, Budapest 1121, Hungary

ARTICLE INFO

Article history:
Received 1 December 2021
Revised 24 February 2022
Accepted 3 March 2022
Available online 4 March 2022

Keywords:
Ethanol
Butadiene
Hard templating
Mesoporous MgO
MgO-SiO_2 catalysts
Acid-base properties

ABSTRACT

Magnesia-silica mixed oxide catalysts of different texture and morphology were prepared for the ethanol-to-butadiene (ETB) reaction. Magnesia of low and high specific surface area (SSA) were made by thermal decomposition of magnesium nitrate. High-SSA MgO was prepared using hard-templating (HT) method. Mesoporous carbon, obtained by carbonizing a resorcinol-formaldehyde polymer was used as template. The carbon pores were saturated by $Mg(NO_3)_2$ solution and calcined then in order to decompose the nitrate and combust the carbon to get high-SSA MgO. The processes induced by latter calcination were followed by Thermogravimetry-Differential Scanning Calorimetry (TG-DSC) method. To obtain MgO-SiO_2 catalysts both magnesia samples were wet-kneaded (WK) with a silica aerogel and a structured mesoporous SBA-15 silica material, having lower and higher SSA, respectively. Morphological and textural properties of these mixed oxide catalysts were characterized by means of N_2 physisorption, X-ray powder diffraction (XRD), Transmission Electron Microscopy (TEM), X-ray photoelectron spectroscopy (XPS), and Energy Dispersive X-ray Spectroscopy (EDX). Ranking the catalysts was attempted according to their acidity and basicity, i. e., by the concentration and strength of their acidic and basic sites. Therefore, the samples were characterized by their adsorption interaction with molecules, having either basic or acidic character. The adsorption of CO_2 and NH_3 was studied by Temperature-Programmed Desorption (TPD) method, whereas that of the pyridine and $CDCl_3$ by Fourier Transform Infrared Spectroscopy (FT-IR). The WK changed the structure of the parent oxides, generated Mg-O-Si bonds, acidity, and basicity. The XPS and EDX results showed that the surface Mg content of the mixed oxide samples made from the low-SSA MgO was higher than that of the bulk phase, while that of the samples made of the high-SSA MgO was lower. This demonstrates that MgO prepared by use of a carbon template proved to be more reactive in the WK process and generated more Mg-O-Si bonds. The mixed oxide catalysts containing high-SSA MgO showed always higher activity and butadiene (BD) selectivity than the corresponding catalyst containing low-SSA MgO. The higher BD selectivity of these catalysts is related to their subtle acidity-basicity balance. Nevertheless, the measured selectivities did not show correlation with any of the parameters characterizing the acid-base properties of the catalysts. The highest BD yield was obtained at 425 °C achieving 75% ethanol conversion level and 50% BD selectivity.

1. Introduction

The 1,3-Butadiene (BD) is one of the most important raw materials of plastics and rubber industries. Today, it is produced almost exclusively on crude oil basis. At the dawn of rubber production only natural rubber was available, having plant-derived BD homologue isoprene (2-methyl-1,3-butadiene) as main component. Because of the rapidly increasing rubber demand research was launched to make synthetic rubber at the beginning of the last century. The ethanol-to-butadiene reaction (ETB) proved to be promising. Two catalytic synthesis processes were elaborated, namely the one-step process (Lebedev synthesis), applying pure ethanol, and the two-step process (Ostromislensky synthesis), using ethanol-acetaldehyde mixture as reactant. However, the growing petroleum industry virtually terminated the application and development of the ETB reaction in the 1950s. Driven by carbon neutrality requirements and rapidly growing bioethanol produc-

* Corresponding author.
E-mail address: barthos.robert@ttk.hu (R. Barthos).

https://doi.org/10.1016/j.molstruc.2022.132764

tion, the interest in the ETB reaction increased and its research gained momentum in the last twenty years. Two reaction pathways were suggested for the reaction. According to the widely accepted one first acetaldehyde is formed, then two acetaldehyde molecules combine to 3-hydroxybutanal. From latter compound crotonaldehyde is formed by dehydration. The crotonaldehyde is hydrogenated to crotyl alcohol by Meerwein–Ponndorf–Verley (MPV) reduction [1]. Another opinion is that crotyl alcohol is formed from the direct reaction of ethanol and acetaldehyde co-adsorbed on the surface of the catalyst [2,3]. BD is obtained from the crotyl alcohol in a final dehydration step. The co-operation of the acidic and basic sites is required for the reaction to proceed in the correct direction. Several papers have recently been published explaining the conversion of glycerol to, for example, ethanol [4], allyl alcohol [5] and glycidol [6] through the concerted action of acidic/basic sites.

The most commonly used catalysts (supports) in the ETB reaction are MgO-SiO_2 [3,7–25] and ZrO_2-SiO_2 [26,27]. In the reaction pathways described above the acetaldehyde is reactant or primary product. In compliance with this several studies have shown that catalyst additives with ethanol dehydrogenation activity, such as, transition and noble metals or their oxides could significantly increase the BD yields [5,9,10,14,15,17]. However, some studies reported that comparable BD yields were obtained over pure MgO-SiO_2 than over catalysts containing a third metal. Results suggested that the mixing method of the oxide components is of great importance. The acid-base properties of the catalyst and, thereby, its hydrogenation-dehydrogenation, C–C coupling, and dehydration activity depended on the properties of the parent oxides and on the method applied for mixing them. There is no consensus in the literature about the most effective mixing method. Usually higher BD yields were found over catalysts prepared by wet-kneading (WK) method than over those made by simple mechanical mixing [7,24], coprecipitation [12,21,24] or by incipient wetness [24] techniques. Several results demonstrate that the BD yield can be increased by enhancing the specific surface area (SSA) and porosity of the silica component of the MgO-SiO_2 mixed oxides. Thus, various mesoporous, high-SSA silicas were used, such as SBA-15 [10,13,27], MCM-41 [27], TUD-1 [28,29], dealuminated BEA [27,30] etc., which were then combined with MgO or metals/metal-oxides in different ways. However, less attention is given to increasing the SSA and porosity of MgO. Miyaji et al. [31] showed that the hydrothermal treatment of calcined MgO modified the structure of MgO and increased its SSA. As a result the hydrothermally treated MgO had increased butadiene selectivity. Men et al. [9] used polyvinylpyrrolidone as soft template to increase the SSA and porosity of MgO, whereas Reschetilowsky et al. [14] applied hydrothermal treatment of magnesium nitrate in the presence of alkali metal carbonates to prepare MgO of high-SSA. Another method of preparing high-SSA mesoporous MgO is the so-called hard-templating (HT) process, in which the magnesium precursor is introduced into the pores of mesoporous carbon from which mesoporous MgO is formed by calcination treatment [32]. The most widely used carbons for the HT process are CMK-3 [33] and carbon obtained by thermal decomposition of resorcinol/formaldehyde polymer [32,34–36].

The present study aims to understand the effect of SSA and porosity of MgO and SiO_2 components on the ETB activity of MgO-SiO_2 catalysts, prepared by WK.

2. Experimental

2.1. Catalysts

Four magnesia-silica mixed oxides and four parent oxides were studied. A lower-SSA silica aerogel was prepared and a higher-SSA structured mesoporous SBA-15 silica material was also used. These materials are designated as Si_L and Si_H, respectively. Also a lower-SSA and a higher-SSA magnesia were prepared and designated as Mg_L and Mg_H, respectively. The mixed oxides made by WK from these oxides are identified as Mg_L-Si_L, Mg_L-Si_H, Mg_H-Si_L, and Mg_H-Si_H.

Silica hydrogel was obtained by dropwise adding of 41.6 g of tetraethyl orthosilicate (TEOS) to 440 ml of 3 to 1 mixture of ethanol-NH_3 solution at 70 °C. The mixture was stirred overnight then the solvent was evaporated at 70 °C. The residue was dried at 120 °C for 12 h and calcined at 550 °C to get the silica aerogel, Si_L.

The Si_H is a commercial SBA-15 product, purchased from Nanjing XFNANO Materials Tech Co., Ltd., China. Prior use this material was dried at 120 °C.

The Mg_L was obtained by thermal decomposition of $Mg(NO_3)_2{\cdot}6H_2O$. The nitrate was heated up in air to 600 °C at a rate of 1 °C/min and kept at the final temperature for 8 h.

The Mg_H sample was prepared by the HT method. In the first step a resorcinol-formaldehyde (molar ratio 2) polymer was synthesized: 97 g of resorcinol and 143 g of formaldehyde (aqueous solution, containing about 37 wt% formaldehyde, stabilized with 10 vol% methanol) were mixed in 260 g of water. To the solution 0.1875 g of Na_2CO_3, pre-dried at 120 °C, was added to initiate polymerization. The mixture was then aged at room temperature for one day and then kept at 50 °C for 48 h and at 90 °C for a further 192 h in an oven. To remove the water from the pores the product was four times washed with 1500 mL of acetone then dried for 24 h at room temperature. The polymer was carbonized in a tube furnace. It was flushed by an N_2 flow of 200 ml min^{-1} and heated up to 800 °C at a heating rate of 1 °C min^{-1}. The material was kept at this final temperature for additional 5 h. In the next step the obtained carbon (60 g) was soaked in $Mg(NO_3)_2$ solution (1200 mL, 3.5 M) for seven days. Then filtered over G1 sintered glass filter, dried at room temperature overnight, and then at 120 °C for 48 h. A mesoporous magnesium oxide (Mg_H) was obtained by calcining the dried product in air. The temperature was raised to the final calcination temperature of 600 °C at a rate of 1 °C min^{-1} and the preparation was kept at this temperature for 8 h.

WK was performed by stirring mixtures of 2.68 g MgO and 2.00 g SiO_2 (the Mg/Si molar ratio equals 2) in 100 mL water for 5 h at room temperature then the water was evaporated, the solid residue was dried at 120 °C overnight and calcined then at 550 °C for 5 h.

2.2. Catalyst characterization

The thermochemical transformations of the resorcinol-formaldehyde polymer, the mesoporous carbon, and the $Mg(NO_3)_2$-soaked carbon were followed using Setaram LabsysEvo (Lyon, France) TG-DSC system. Samples were weighed into an Al_2O_3 crucible having 100 µL volume. The reference crucible was kept empty. The polymer was heated up to 800 °C in flowing high purity nitrogen (99.999%), whereas the other two preparations in a flow of synthetic air to 600 °C. The gas flow rate was always 80 mL min^{-1} and the heating rate was 5 °C min^{-1}. The obtained curves were baseline-corrected and further processed with the processing software of the thermoanalyzer (Calisto Processing, ver. 2.092, AKTS, Switzerland). Both the temperature scale and the calorimetric sensitivity of the analyzer was calibrated by a multipoint calibration method, in which seven different certified reference materials were used to cover the operating temperature range.

X-ray powder diffractograms were recorded at room temperature using a Philips PW 1810/3710 diffractometer, applying monochromatized CuKα (λ =0.15418 nm) radiation (40 kV, 35 mA) and proportional counter. Data were collected at room temperature

between 1.5° and 70° 2θ, in 0.04° steps, counting signals for 0.5 s in each step.

Nitrogen adsorption/desorption isotherms were measured using Thermo Scientific Surfer automatic, volumetric adsorption analyzer at 77 K. Prior to the measurements the samples were evacuated for 2 h at 250 °C.

The morphology of the samples was examined by a Thermofisher Themis 200 Cs-corrected (scanning) transmission electron microscope (S)TEM with an accelerating voltage of 200 keV. EDX maps were recorded using Super-X EDX detectors in STEM mode.

X-ray photoelectron spectroscopy (XPS) measurements were carried out by a Kratos XSAM 800 spectrometer operating in fixed analyzer transmission mode, using Mg $K\alpha_{1,2}$ (1253.6 eV) excitation. Survey spectra were recorded in the kinetic energy range of 100–1300 eV with 0.5 eV steps. High resolution spectra of the main constituent elements (O1s, C1s, Si2p, Mg2s) were recorded by 0.1 eV steps. Spectra were referenced to the C1s line (284.6 eV binding energy) of the hydrocarbon type carbon contaminant. Quantitative analysis, based on peak area intensities after removal of the Shirley type background, was performed by the Kratos Vision 2 and by the XPS MultiQuant programs [37], using experimentally determined photoionisation cross-section data of Evans et al. [38] and asymmetry parameters of Reilman et al. [39]. Surface chemical compositions were calculated by the "infinitely thick sample" model. Correction for surface contamination was done by the method of Mohai [40].

Acid-base properties of the samples were determined by NH_3 and CO_2-TPD and by recording the FT-IR spectra of adsorbed pyridine and $CDCl_3$.

For NH_3-TPD measurements the samples, filled in a U-tube quartz reactor, were pre-treated in a 30 ml min^{-1} flow of O_2 at 500 °C for 1 h, then flushed by N_2 (30 ml min^{-1}) at the same temperature for 15 min. The pre-treated sample was evacuated at 550 °C, cooled to room temperature and contacted with NH_3 at about 14 kPa pressure. After 15 min the weakly adsorbed ammonia was removed by evacuation. Then the reactor temperature was ramped up in He flow (20 ml min^{-1}) at a rate of 10 °C min^{-1} to 150 °C. After holding this temperature for 30 min, the sample was heated up to 550 °C (10 °C min^{-1}) and held at this temperature for 1 h. The effluent gas was passed through a dry ice-acetone trap and a thermal conductivity detector (TCD).

CO_2-TPD measurements were also performed as described above, omitting the isothermal step at 150 °C.

Calculation of the adsorbed amount of both probe molecules was based on the peak areas. Prior to the measurements the TCD was calibrated by passing through it known amounts of NH_3 or CO_2.

The FT-IR spectra were recorded by a Nicolet Impact Type 400 FT-IR spectrometer. Always 64 scans were averaged at a resolution of 2 cm^{-1}. The self-supporting pellet method and a conventional high-vacuum IR cell were used. The pellets were pre-treated in vacuum at 450 °C for 1 h. In case of pyridine adsorption measurements, the sample pellet was contacted with pyridine at 666 Pa pressure and 200 °C. Spectra were collected at room temperature after successive evacuations at 100, 200, 300, 400, and 450 °C for 30 min. The $CDCl_3$ adsorption measurements were carried out at about 933 Pa adsorptive pressure in the IR cell at room temperature.

2.3. Catalytic activity

Catalytic ETB reaction was carried out at atmospheric pressure in fixed-bed flow-through, quartz tube (Ø = 10 mm) microreactor. The catalysts (~ 1 g, particle size 0.315–0.65 mm) were activated in oxygen flow (20 ml min^{-1}) for 30 min at 550 °C. Ethanol was introduced into an evaporation zone in front of the catalyst bed using a Gilson 307 HPLC Piston Pump. The composition of the feed was ~15% ethanol/He at a total flow rate of 30 ml/min (0.5 $g_{ethanol} \cdot g_{cat}^{-1} \cdot h^{-1}$) and the reaction temperature was varied for measuring the temperature dependence of the activity. The effect of contact time was analyzed by using the same reactant concentration and changing of the total flow rate between 7.5 and 180 mL min^{-1}. The reaction products were analyzed by on-line gas chromatograph (GC) (Shimadzu GC-2010). The GC was equipped with two FID detectors. One was connected to a Chrompack PLOT Fused Silica column with Al_2O_3/KCl stationary phase (50 m long, 0.32 mm diameter) for the analysis of hydrocarbon products, while the other one was connected to a HP- PLOT-U column (30 m long, 0.32 mm diameter) for the analysis of oxygenates. The GC was calibrated for ethanol and for all major products in independent measurements.

The conversion was calculated from the difference between the amount of ethanol fed and the amount of unreacted ethanol. The product selectivity was defined as the ratio of the carbon atom number of a product and the summarized carbon atom number of all the products.

3. Results and discussion

3.1. TG-DSC characterization of mesoporous carbon production

Carbonization of the resorcinol-formaldehyde polymer was carried out in N_2 flow applying a temperature ramp-up from 25 to 800 °C. The weight loss in this carbonization process was 51.07 wt% (Fig. 1A). On the DSC curve two endothermic peaks appeared. The low-temperature peak (40–120 °C, heat flow onset temperature of 48 °C) belongs to desorption of acetone/water, while the high-temperature peak (450–630 °C, heat flow onset temperature of 464 °C) can be attributed to condensation and decomposition of the resorcinol phenolic hydroxyl groups. The decomposition/combustion of mesoporous carbon and the decomposition/combustion of $Mg(NO_3)_2$-soaked carbon was carried out by raising the temperature of the sample from 25 to 600 °C in air flow. The conversion of the mesoporous carbon started around 420 °C and the weight loss was 84.50 wt% at the end of the heating up procedure. It should be mentioned that the tailing of the TG curve suggests that the combustion of coal is not complete at this temperature. Note that in this measurement there was no further isothermal treatment at the highest temperature. The heat effect of the carbon combustion, evaluated from the DSC curve, was –14.4 kJ g^{-1} with heat flow onset temperature of 469 °C. The peaks in the high temperature range of the TG curve can be explained by the flaring of carbon particles Fig. 1.C demonstrates that the presence of $Mg(NO_3)_2$ promotes carbon combustion. It started at lower temperature and there was no weight loss above 480 °C. The total weight loss was 84.70 wt%. The amount of the formed high-SSA MgO was calculated to be around 15 wt% of the $Mg(NO_3)_2$ soaked carbon. The heat effect of $Mg(NO_3)_2$ decomposition and carbon combustion was −18 kJ/g with heat flow onset temperature of 359 °C.

3.2. Structure and morphology

The XRD patterns of all mixed oxide samples (Fig. 2A) show a broad diffraction line at around 2Θ = 20–30°, attributed to amorphous SiO_2, and lines of the periclase modification of MgO at 2Θ = 43.0 and 62.5° It can also be observed that in case of the Mg_L samples the lines belonging to MgO are somewhat stronger and narrower, suggesting a higher degree of crystallinity. A reflection at around 35.3° could be discerned in the X-ray patterns of the mixed oxide samples except in the pattern of the low-SSA Mg_L-Si_H

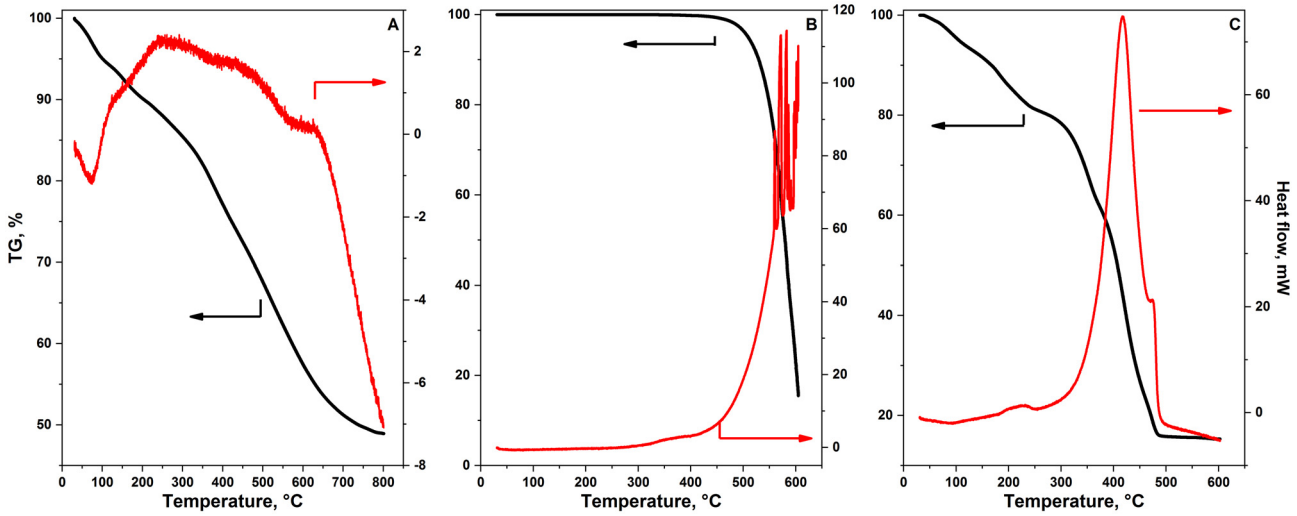

Fig. 1. TG (left axes)-DSC (right axes) decomposition curves of (A) resorcinol-formaldehyde polymer, and decomposition/combustion of (B) mesoporous carbon, and (C) $Mg(NO_3)_2$ soaked carbon in (A) flowing nitrogen and (B, C) in air at 80 ml min^{-1} gas flow, and 5 °C min^{-1} heating rate.

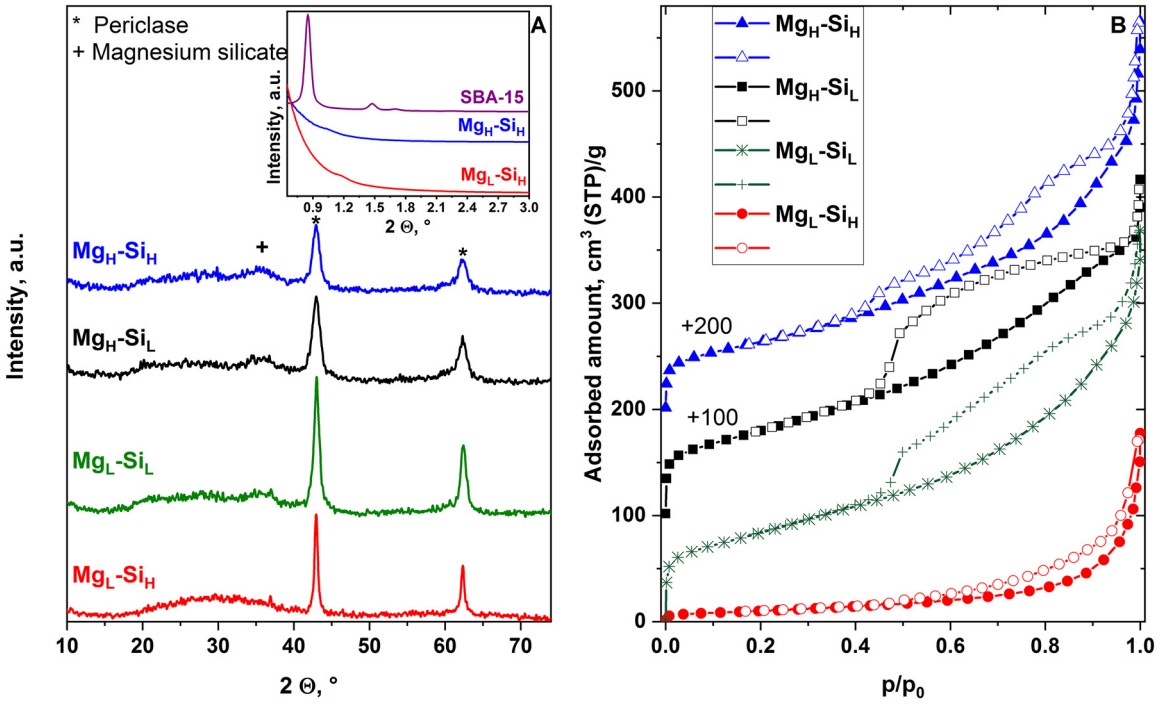

Fig. 2. (A) XRD patterns and (B) N_2 adsorption-desorption isotherms at −196 °C of the samples. Adsorption and desorption branches are indicated by full and open symbols, respectively. The insert in (A) shows the low-angle 2Θ region of the XRD pattern of SBA-15 and SBA-15-based catalysts.

preparation. This reflection substantiates the presence of magnesium silicate in the catalysts.

Because acid-base properties stem from the electronic disbalance of Mg-O-Si bonds the ETB activity of the catalyst is strongly related to the surface concentration of such bonds. The crystallite size, calculated by the Scherrer equation from the XRD diffraction peaks of MgO suggests that the magnesia particles were degraded during the WK process (Table 1).

The nitrogen physisorption isotherms (Fig. 2B) show that the Si_L in the mixed oxide catalysts retained the characteristics of the parent Si_L (The isotherms of the parent materials are shown in the Supporting Information, Fig. SI1). The shape of the hysteresis loop indicates that these samples contain mesopores of broad size distribution. The SSA of the Si_L material and the catalysts, containing Si_L are similar (near to 300 m^2/g). It can be concluded that the added MgO did not significantly affect the morphology of the parent Si_L silica (Table 1). However, the isotherms of the Si_H-containing catalysts suggest that the structure of the parent SBA-15 material has changed significantly during the WK procedure. The isotherm of the Mg_H-Si_H sample shows flattened and spread hysteresis loop in the relative pressure range of 0.40–0.95 (Fig. 2B). The pore volume and size were also significantly reduced relative to those of the parent SBA-15 material (Table 1). These results suggest that the ordered SBA-15 structure has partially collapsed, moreover, some mesopores could have been clogged by MgO particles. The structural change was the most pronounced for the Mg_L-Si_H catalyst, wherein the original structure of the parent SBA-15 has been completely collapsed or the pores of the parent SBA-15

Table 1
Textural and acid-base properties of magnesia-silica catalysts, prepared by the wet kneading method, and their parent low and high SSA oxides.

Sample	Textural properties				Acidic properties			Basic properties		
	SSA[a]	PV[b]	PD[c]	CS[d]	c_a (w)[e]	c_a (m)[f]	Pyridine[g]	c_b[h]	$CDCl_3$ (w)[i]	$CDCl_3$ (m)[j]
Mg_L	5	0.03	5.56	82	4/0.8	–	0.05	67/13.4	0.44	0.63
Mg_H	53	0.34	20.29	27	119/2.25	132/2.49	0.09	8/0.15	0.91	–
Si_L	300	0.39	4.30	–	64/0.21	–	0.05	1/0.00	0.24	–
Si_H	494	1.20	8.09	–	–	–	0.12	–	0.10	–
Mg_L-Si_L	299	0.48	3.88	14	143/0.48	91/0.30	0.63	35/0.12	0.82	0.6
Mg_L-Si_H	39	0.19	3.96	23	52/1.33	39/1.00	0.16	17/0.44	0.49	–
Mg_H-Si_L	287	0.40	4.26	10	221/0.77	156/0.54	0.59	31/0.11	0.74	1.35
Mg_H-Si_H	233	0.44	3.37	10	169/0.73	143/0.61	0.91	32/0.14	0.63	0.89

[a] specific surface area (m^2/g).
[b] pore volume calculated by the Gurvich method (cm^3).
[c] most frequent pore diameter calculated from the desorption branch by the BJH method (nm).
[d] crystallite size of MgO calculated by the Scherrer equation (nm).
[e] adsorbed amount of NH_3 (μmol/g)/(μmol/m^2); amount of sites, having weak acid strength.
[f] adsorbed amount of NH_3 (μmol/g)/(μmol/m^2); amount of sites, having medium acid strength.
[g] integrated area of FT-IR band at around 1448 cm^{-1} after evacuation at 200 °C.
[h] adsorbed amount of CO_2 (μmol/g)/(μmol/m^2).
[i] integrated area of the peak at around 2257 cm^{-1}, obtained from the adsorption of $CDCl_3$ at room temperature; the peak area represents the amount of sites, having weak base strength.
[j] integrated area of the peak at around 2230 cm^{-1}, obtained from the adsorption of $CDCl_3$ at room temperature; the peak area represents the amount of sites, having medium base strength.

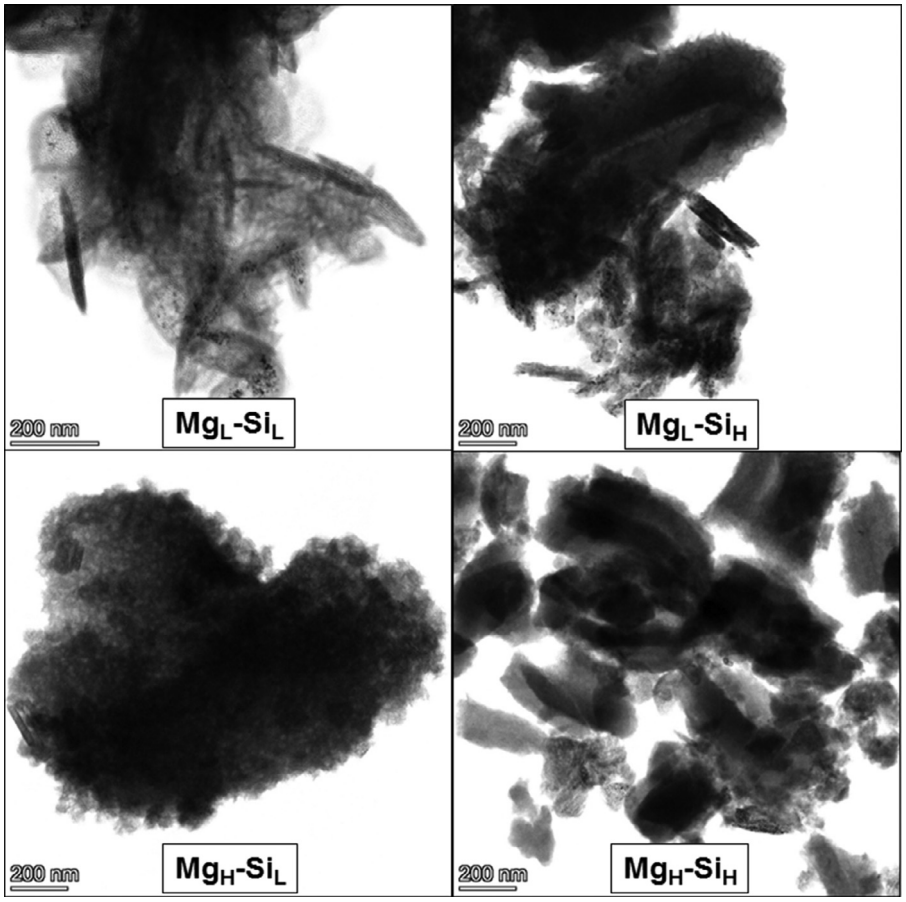

Fig. 3. TEM images of the samples.

are totally blocked. The obtained mixed oxide had an SSA as low as 39 m^2/g which is a very typical value for external surface area of SBA-15 silica particles. The small-angle XRD patterns (insert in Fig. 2A) show that the original regular structure disappeared due to WK process. Nevertheless, the sample retained some mesoporosity.

The TEM images, shown in Fig. 3 suggest that the catalysts are morphologically inhomogeneous. The elemental maps of the samples prove that the samples consist of crystalline MgO, and amorphous Si-Mg-O-containing phases. The catalysts produced by WK using low-SSA MgO contain crystalline MgO particles, having a diameter of around 300–500 nm, as well as, 100–200 nm long needle-like MgO crystals. In accordance with the results of XRD measurements these samples exhibit higher degree of crystallinity than the samples made from high-SSA MgO. In latter catalysts the crystalline MgO particles are smaller (Ø=100–200 nm) and no or only very few needle-like MgO crystallites can be observed.

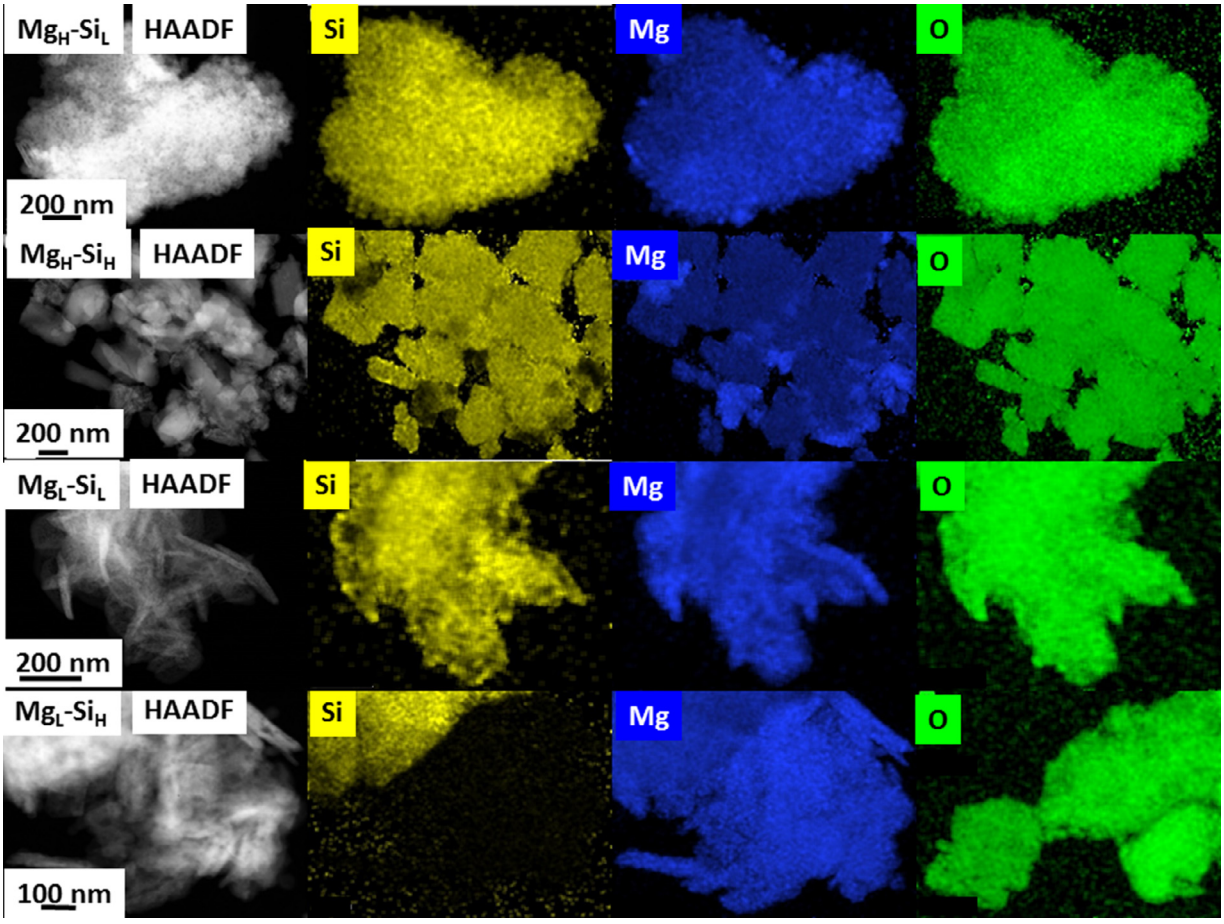

Fig. 4. Elemental maps of the catalysts. HAADF: High-Angle Annular Dark-Field imaging.

The elemental maps of the samples are shown in Fig. 4. The map of the Mg_H-Si_L sample shows that the distribution of the two components in this sample is quite homogeneous. In contrast, most SiO_2 particles in the Mg_H-Si_H mixed oxide catalyst and in the catalysts, containing Mg_L are coated with MgO particles (and vice versa). This is indicated by the fading of the elemental map. The conclusions drawn for the structures of the catalysts from the analysis of their N_2 adsorption isotherms are in harmony with above findings.

The Mg/Si ratio used in the synthesis was 2/1. For determining the surface Mg/Si ratios of the catalysts XPS measurements were performed. The surface of the samples, containing low-SSA MgO was enriched in Mg (Mg/Si>2), whereas the surface Mg/Si ratio of the samples, containing high-SSA MgO were smaller than 2. The Mg/Si ratios were also determined from EDX measurements. Although this method is less accurate than the XPS method, similar results were obtained than by XPS (Fig. 5). The oxygen peaks were deconvoluted into three components, but no physical meaning could be assigned to these peaks and no significant difference can be recognized for these components (Table SI1).

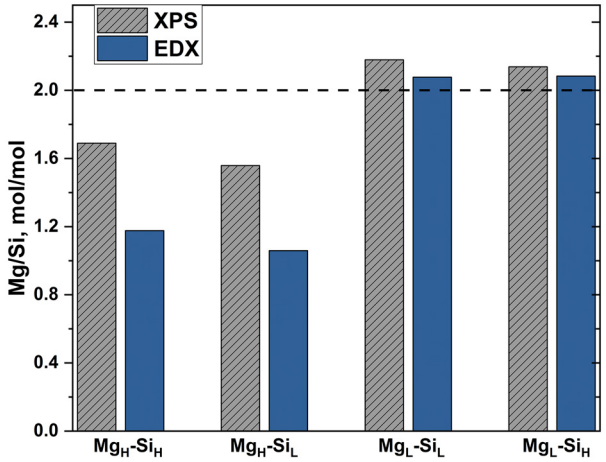

Fig. 5. Surface Mg/Si ratios of the catalysts determined by XPS and EDX methods. The straight line indicates the 2 to 1 molar ratio, used for synthesis.

3.3. Acid-base properties

The results derived from the TPD (Fig. 6, Fig. SI2) and the FT-IR (Fig. 7, Fig, SI3) measurements are given in Table 1.

In the NH_3-TPD measurements an isothermal step was applied at 150 °C for about 30 min to desorb the weakly adsorbed ammonia (Fig. 6A). The ammonia, desorbed in this period and at temperatures <150 °C was assigned to sites of weak acid strength, whereas the ammonia, desorbed at higher temperatures was assigned to sites of medium acid strength. The results show that more acid sites are in the mixed oxide samples containing Mg_H than in those containing Mg_L, while the acid strength of the sites is nearly the same.

We could come to similar conclusions from the pyridine adsorption measurements. The IR spectra shows that adsorbed pyridine is coordinated to Lewis acid sites. Bands of surface-bound protonated pyridine were not discernible. These results suggest that catalysts are Lewis acids and do not have Brønsted acidity. The

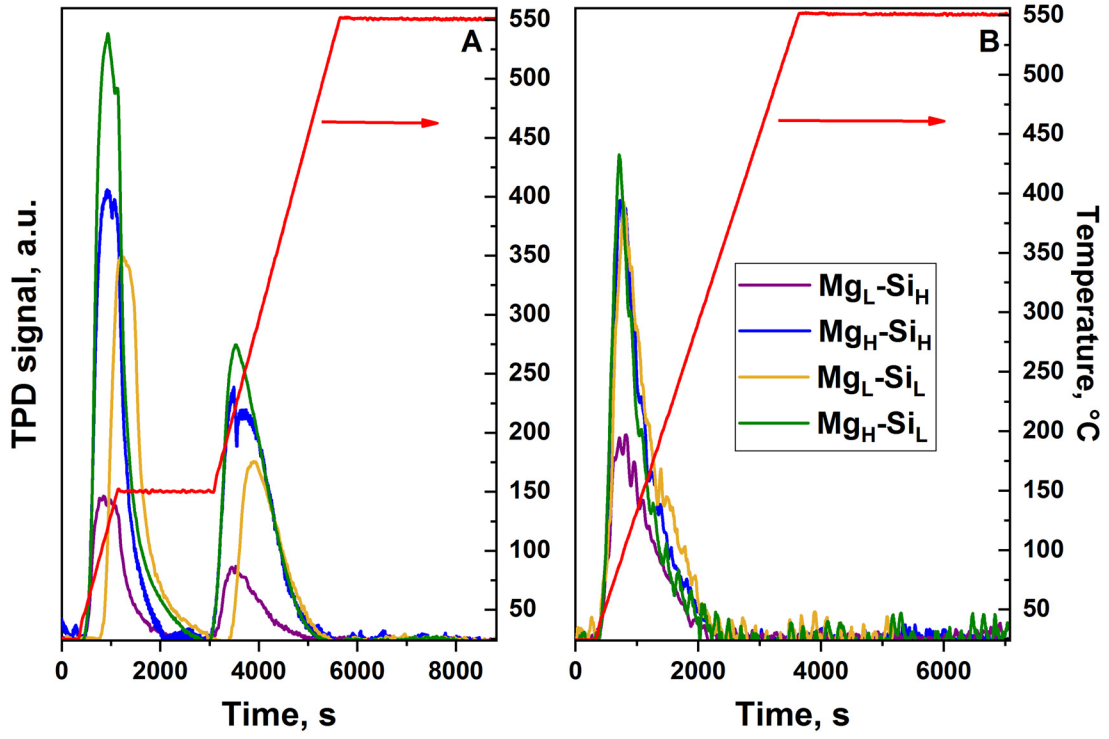

Fig. 6. TPD curves of (A) NH_3 and (B) CO_2 of the mixed oxide preparations.

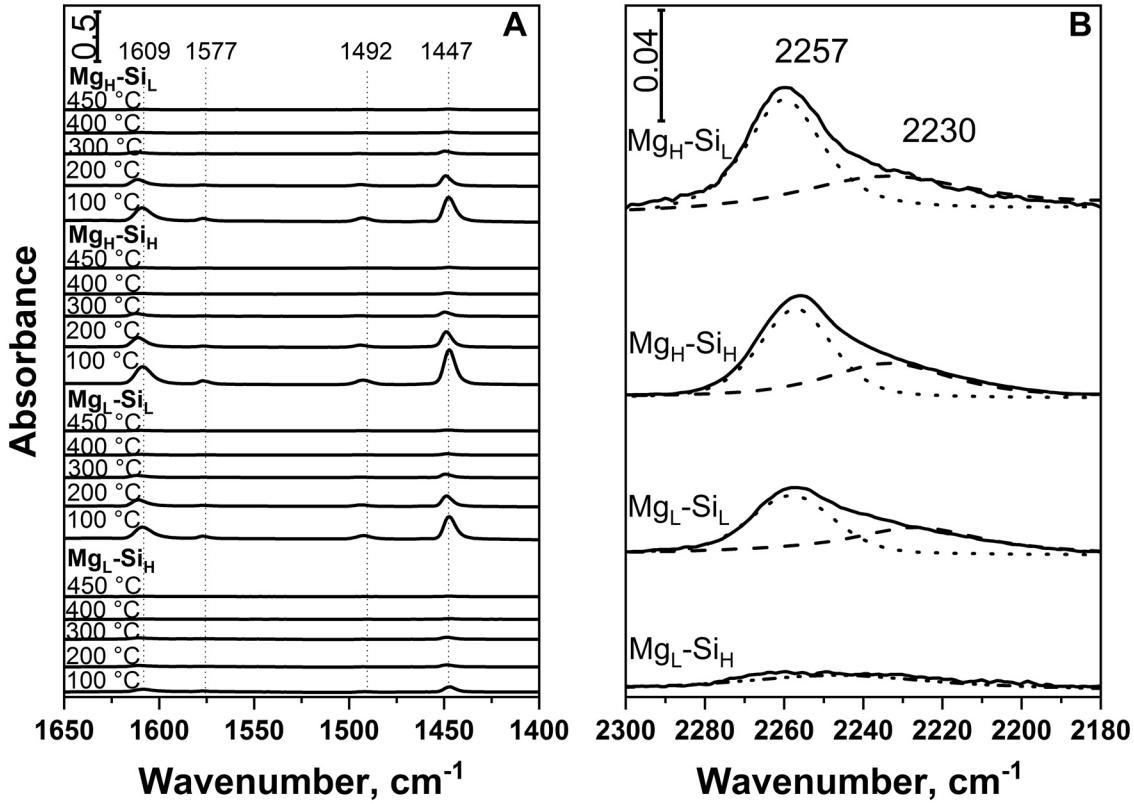

Fig. 7. Room-temperature FT-IR spectra of adsorbed (A) pyridine (666 Pa) after 30 min successive evacuation of the sample at the indicated temperatures and (B) $CDCl_3$ (933 Pa) in presence of adsorptive gas in the cell. Before the adsorption each pellet was activated at 450 °C for 1 h.

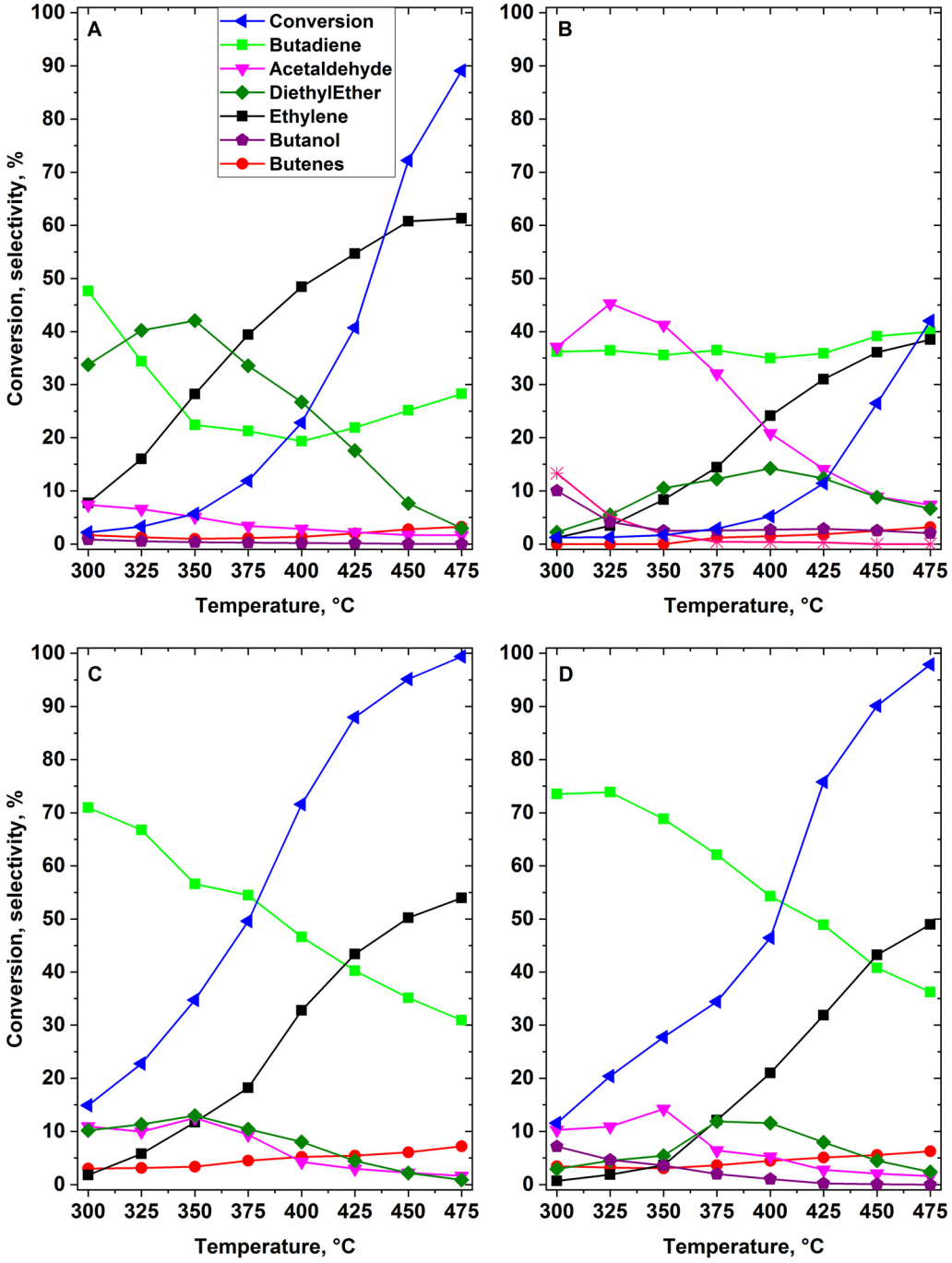

Fig. 8. Catalytic conversion of ethanol/He mixture at atmospheric pressure as function of reaction temperature over (A) Mg_L-Si_L, (B) Mg_L-Si_H, (C) Mg_H-Si_L, (D) Mg_H-Si_H catalysts using flow-through microreactor. The WHSV and the partial pressure of ethanol were 0.5 $g_{ethanol} \cdot g_{cat}^{-1} h^{-1}$ and about 15 kPa, respectively.

amount of the Lewis acid sites was indicated by the amount of pyridine that could be retained by the catalyst at a given evacuation temperature. The Mg_H-Si_H catalyst contains more acid sites than the Mg_H-Si_L and Mg_L-Si_L samples, because the Mg_H-Si_H catalyst retained more pyridine after evacuation at 200 °C than the other two preparations (Fig. 7A, Table 1). However, when the IR peak area values of the pyridine, retained at different temperatures were normalized to the peak area obtained after evacuation 100 °C, it was found that the strength of the acid sites of the Mg_H-Si_H, Mg_H-Si_L and Mg_L Si_L samples was nearly the same. This is in accordance with the results of the NH_3-TPD examinations (Fig. SI4). It can also be observed that the Mg_L-Si_H sample having low SSA contains significantly less acidic sites than the other three samples. Since this sample bound very small amounts of pyridine already even at 100 °C, normalization probably erroneously indicates that this catalyst would contains the strongest acid sites.

Regarding the basicity of the mixed oxide catalysts, it can be concluded that the catalysts, having Mg_H as magnesia component, contain sites of stronger basicity then the catalysts containing Mg_L. In a previous work [9] we have shown that the ν_{CD} frequency $CDCl_3$ molecules were shifted from 2260 cm^{-1} to lower wavenumbers if the molecule was in interaction with basic surface sites. The band displacement reflects the strength of interaction and, thereby, the base strength of the adsorbing surface sites. The integrated

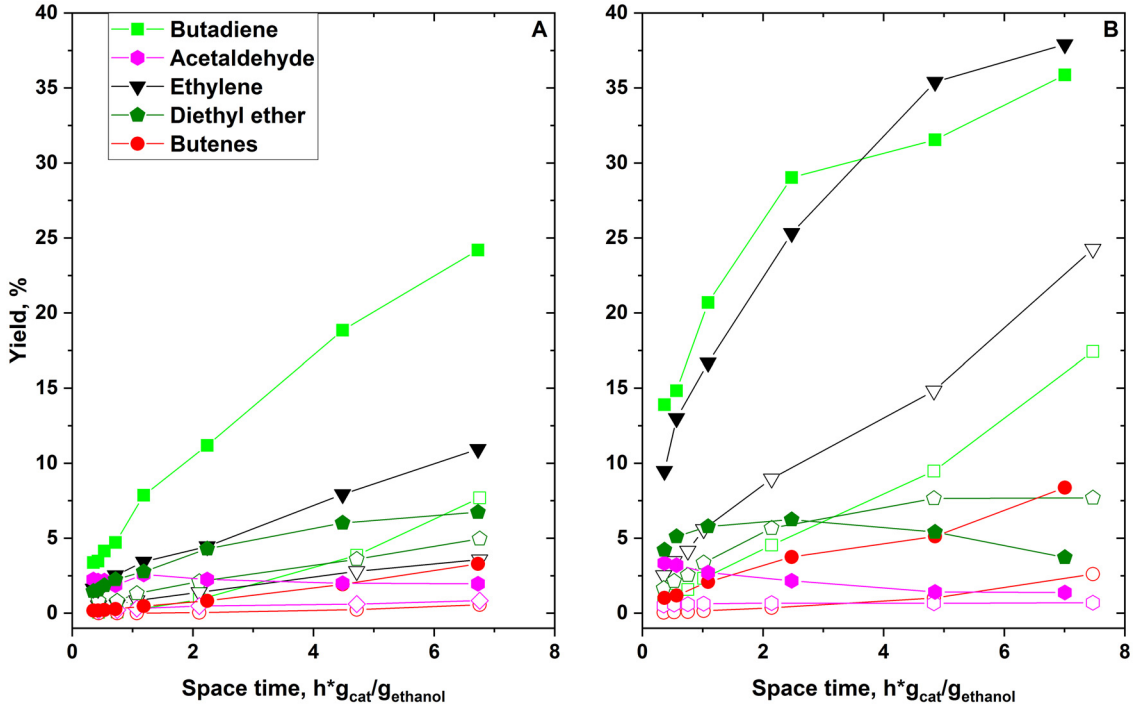

Fig. 9. Effect of space time on conversion of ethanol/He mixture at atmospheric pressure over (A) Mg_H-Si_H (full symbols) and Mg_L-Si_L (open symbols) catalysts at 350 °C, and (B) at 400 °C. The WHSV of ethanol was varied between 0.2 and 3.0 $g_{ethanol} \cdot g_{cat}^{-1} h^{-1}$ at about 15 kPa partial pressure.

band area gives an approximate measure of the amount of adsorption sites. The peaks resolved at 2257 cm^{-1} and at 2230 cm^{-1}, were assigned to $CDCl_3$, bound to surface sites having weak or by medium base strength, respectively. (Fig. 7B, and Table 1).

It was also observed that the CO_2-TPD measurements could not differentiate the basicity of the Mg_L-Si_L, Mg_H-Si_L and Mg_H-Si_H samples, as all three showed adsorbed amounts between 32 and 35 µmol/g (Fig. 6B, Table 1). In general, the use of MgO, having high-SSA in WK procedure favors the formation of Mg-O-Si bonds and thus the formation of moderately strong basic and acidic sites.

3.4. Catalytic ETB reactions

Fig. 8 shows the activity of the MgO-SiO_2 mixed oxide catalysts in ETB reaction in the temperature range of 300–475 °C. At reaction temperatures between 300 and 400 °C more than 95% of the carbon fed in the reactor appears in the products, which were measured quantitatively. At higher temperatures (and conversions) the calculated balance gradually declined to about 90% due to appearance of minor products, such as hexadienes, hexatrienes, higher polyolefins, aromatics, hexanols, and octanols, which were neglected in the balance calculation. (Fig. SI5). Over catalysts, containing high surface area MgO (Figs. 8, C and D) BD was formed with higher selectivity compared to the BD selectivity of catalysts, containing low surface area MgO (Figs. 8, A and B). The Mg_L-Si_L catalyst showed the lowest BD selectivity, that varies near to 25% above 325 °C. The low BD selectivity is coupled with a high dehydration activity. The summarized selectivity of ethylene and diethyl ether is close to 70% at temperatures above 350 °C. The Mg_H-Si_L catalyst shows virtually constant BD selectivity of 35–40% in the whole range of applied reaction temperature (Fig. 8B). The dehydration activity of this sample is lower than that obtained for catalyst Mg_L-Si_L, and is similar to the other two catalysts. It can also be observed that significantly lower conversion and higher acetaldehyde selectivity were found on this Mg_H-Si_L catalyst. Samples Mg_H-Si_L and Mg_H-Si_H show very similar catalytic behavior, but the BD selectivity of the Mg_H-Si_H catalyst is about 5 to 10% higher at each temperature and reaches 55–65% in temperature range of 350–400 °C.

Comparing the effect of space-time on the ETB activity of Mg_L-Si_L and Mg_H-Si_H catalysts at 350 and 400 °C (Fig. 9) it can be concluded that significantly higher BD yields were achieved on catalysts which are composed from high-SSA components. When the space-time was increased the ethanol conversion and the yields of main products (BD, ethylene, diethyl ether) increased. Over the Mg_H-Si_H catalyst about 25 and 35% BD yields were achieved at 350 and 400 °C, respectively. The higher residence time of the reactant favors the formation of ethylene, however over Mg_H-Si_H sample at 350 °C the yield of the BD was higher than that of the ethylene in the whole applied space time range (Fig. 9B). The space time dependence of ETB activity was determined for all the four studied mixed oxide catalysts. The conversion curves are given as Supporting Information. (Figs. SI6 and SI7). The catalyst selectivities were compared at two temperatures and ethanol conversions (350 °, 10% and 400 °C, 40%) (Fig. 10). The four catalyst preparations have different SSA and, because of the differences in the surface composition and structure, different adsorption and catalytic properties. In other words, besides the temperature, the reaction rates and the steady-state conversions are determined by the intrinsic rate constants (k) of the proceeding reactions, the adsorption equilibrium constants (K) of the reactants and products, a wall as, the number of active sites of each reaction, which latter is most related to the SSA of the catalysts. The weight hourly space velocity (WHSV) has to be adjusted to compensate the variance of these factors and to get about the same conversion over each catalyst. The catalytic selectivities are sensitive to the structure and composition of the surface of the catalysts. At the same conversion the higher selectivity of a product means also that it is obtained also with a higher yield. Nevertheless, from practical point of view the catalyst should be compared not the by the BD yield but by the BD productivity, i. e., by the arithmetical product of the yield and the WHSV. It is no surprise that at both reaction temperatures those magnesia-silica

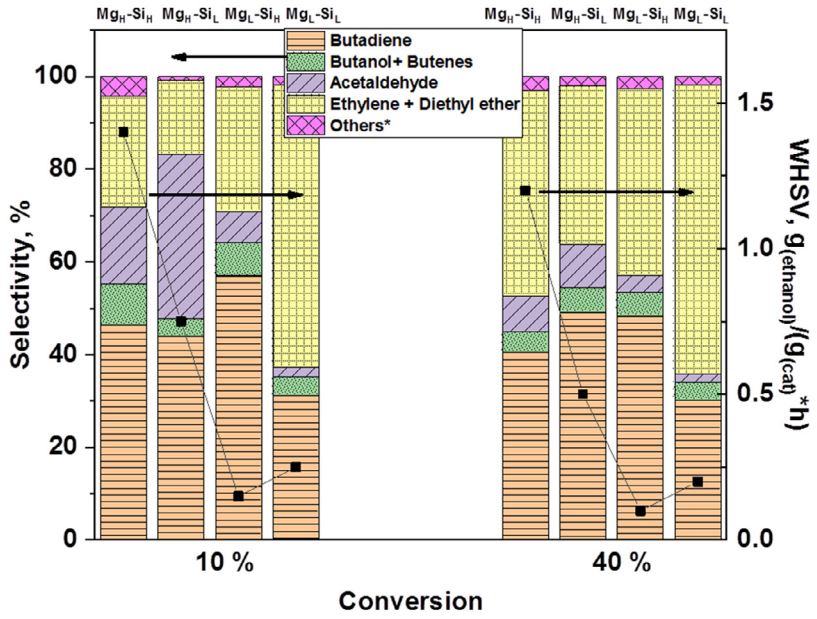

Fig. 10. Effect of the ethanol conversion on the selectivity of the reaction products. The reaction temperatures were 350 °C and 400 °C to achieve 10 and 40% conversion levels, respectively. The WHSV of ethanol was varied between 0.1 and 1.5 $g_{ethanol}\ g_{cat}^{-1} h^{-1}$ at about 15 kPa partial pressure. *Others: methane, ethane, propylene.

catalysts were the most BD productive that contained Mg_H. The catalysts, containing Mg_L are much lower BD productivity regardless of the BD selectivity and the nature of the silica component. The ethylene selectivity was higher at higher temperature. It could increase only on the expense of the selectivity of other products. The decrease of acetaldehyde selectivity is the most pronounced, indicating that the temperature sensitivity of the ethanol dehydration to ethylene is higher than that of ethanol dehydrogenation to acetaldehyde. The suppressed production of acetaldehyde is the most probable reason of the decreased selectivity of the C_4 products, including BD at higher temperature (Fig. 10). The selectivities and productivities did not show any correlation with the measured acid-base characteristics of the catalysts (Table 1). Predominantly the structure and properties of the magnesia component, such as, specific surface area, and the reaction temperature direct the ETB reaction over the magnesia and the properties of the silica component has only secondary importance.

Analyzing the effect of the acidity/basicity of the catalysts on the catalytic activity, it can be concluded that the samples containing more acid/base pair sites of medium strength show higher BD selectivity. The relatively stronger basicity can be linked to the presence of high SSA MgO, which favors the coupling reaction, while the moderately strong acid sites, stemming from Mg-O-Si bonds, promote the selective dehydration of crotyl alcohol to BD, and suppresses the undesired formation of ethylene and diethyl ether. The development of favorable catalytic properties can be explained by the fact that the MgO prepared by use of a carbon template is more reactive in the WK process and more Mg-O-Si bonds are formed. In addition, the sample made of MgO with a high specific surface area is itself more active in the coupling reactions and retains some of this property after the WK process. It can also be concluded that higher BD selectivities can be achieved with any WK-prepared magnesia-silica mixed oxide catalysts, regardless of the SSA of the applied MgO component, if the silica component has higher SSA.

4. Conclusions

In this study four MgO-SiO_2 catalysts were prepared by the wet kneading (WK) method using high and low specific surface area (SSA) oxides as starting materials. The mixed oxides were characterized and used in the catalytic conversion of ethanol to butadiene. Low and high-SSA MgO were prepared by thermal decomposition of $Mg(NO_3)_2{\cdot}6H_2O$. The high-SSA MgO was obtained by applying the mesoporous carbon assisted hard templating method. The lower and higher-SSA silica materials were silica aerogel and SBA-15 material, respectively. The morphological studies showed that WK led to structural degradation of the parent oxide components. The pore structure of the SBA-15 material was fully destroyed during WK with low-SSA MgO, whereas its WK with high-SSA MgO resulted only in partial pore clogging and some broadening relative to the original pore size distribution of the SBA-15 material. The pore size distribution of the mixed oxides, containing silica aerogel slightly broadened but the samples virtually retained all the textural characteristics of the parent SiO_2. The XRD patterns of the mixed oxide samples show fragmentation of the MgO particles and formation of Mg-O-Si bonds. The XPS and EDX results showed that the surface Mg content of the mixed oxide samples made from low-SSA MgO was higher than that of the bulk phase, while that of the samples made of high-SSA MgO was lower. This suggests that MgO made with the help of a carbon template is more reactive in the WK process than the material produced by thermal decomposition of Mg-nitrate. FT-IR and TPD measurements showed that the mixed oxide samples, prepared using high-SSA MgO contain a higher amount of acid sites and medium strength base sites than the samples made from low-SSA MgO. These findings suggest that the interaction of silica and magnesia promotes the formation of more Mg-O-Si bonds if the magnesia has higher SSA. The high-SSA magnesia in the mixed oxide catalysts has high activity in the acetaldehyde and ethanol-acetaldehyde coupling. Under comparable reaction conditions the mixed oxide catalysts, containing high-SSA MgO, always showed higher butadiene (BD) selectivities than those containing low-SSA MgO. The highest BD yield was reached at 425 °C with 75% ethanol conversion and 50% BD selectivity.

Declaration of Competing Interest

The authors declare that they have no known competing financial interests or personal relationships that could have appeared to influence the work reported in this paper.

CRediT authorship contribution statement

Blanka Szabó: Investigation, Visualization. **Gyula Novodárszki:** Investigation. **Ferenc Lónyi:** Supervision. **László Trif:** Investigation. **Zsolt Fogarassy:** Investigation. **József Valyon:** Supervision. **Róbert Barthos:** Investigation, Supervision.

Acknowledgements

The authors thank to the Ministry of Innovation and Technology of Hungary for financing this study from the National Research, Development and Innovation Fund, under the 2019–2.1.13-TÉT_IN funding scheme (Project No. 2019–2.1.13-TÉT_IN-2020–00043). Thanks are also due to the Interreg V-A Slovakia - Hungary Cooperation Program, SKHU/1902, (Project No: SKHU/1902/4.1/001), and the Competitive Central Hungary Operational Program, VEKOP, supported by the European Union, the State of Hungary, and co-financed by the European Regional Development Fund (Project No. VEKOP-2.3.2–16–2017–00013), and the European Structural and Investment Funds (Project No. VEKOP-2.3.3–15–2016–00002) for supporting this work. One of the authors (Zs. Fogarassy) says thanks also for the support of the János Bolyai Research Scholarship of the Hungarian Academy of Sciences.

Supplementary materials

Supplementary material associated with this article can be found, in the online version, at doi:10.1016/j.molstruc.2022.132764.

References

[1] G. Pomalaza, P. Arango Ponton, M. Capron, F. Dumeignil, Ethanol-to-butadiene: the reaction and its catalysts, Catal. Sci. Technol. 10 (2020) 4860–4911, doi:10.1039/d0cy00784f.
[2] A. Chieregato, J. Velasquez Ochoa, C. Bandinelli, G. Fornasari, F. Cavani, M. Mella, On the chemistry of ethanol on basic oxides: revising mechanisms and intermediates in the Lebedev and Guerbet reactions, ChemSusChem 8 (2015) 377–388, doi:10.1002/cssc.201402632.
[3] J.V. Ochoa, C. Bandinelli, O. Vozniuk, A. Chieregato, A. Malmusi, C. Recchi, F. Cavani, An analysis of the chemical, physical and reactivity features of MgO–SiO_2 catalysts for butadiene synthesis with the Lebedev process, Green Chem 18 (2016) 1653–1663, doi:10.1039/C5GC02194D.
[4] A. Kostyniuk, D. Bajec, B. Likozar, One-step synthesis of ethanol from glycerol in a gas phase packed bed reactor over hierarchical alkali-treated zeolite catalyst materials, Green Chem 22 (2020) 753–765, doi:10.1039/C9GC03262B.
[5] A. Kostyniuk, D. Bajec, P. Djinović, B. Likozar, Allyl alcohol production by gas phase conversion reactions of glycerol over bifunctional hierarchical zeolite-supported bi- and tri-metallic catalysts, Chem. Eng. J. 397 (2020) 125430, doi:10.1016/j.cej.2020.125430.
[6] A. Kostyniuk, D. Bajec, P. Djinović, B. Likozar, One-step synthesis of glycidol from glycerol in a gas-phase packed-bed continuous flow reactor over HZSM-5 zeolite catalysts modified by $CsNO_3$, Chem. Eng. J. 394 (2020) 124945, doi:10.1016/j.cej.2020.124945.
[7] S. Kvisle, A. Aguero, R.P.A. Sneeden, Transformation of ethanol into 1,3-butadiene over magnesium oxide/silica catalysts, Appl. Catal. 43 (1988) 117–131, doi:10.1016/S0166-9834(00)80905-7.
[8] W.E. Taifan, Y. Li, J.P. Baltrus, L. Zhang, A.I. Frenkel, J. Baltrusaitis, Operando structure determination of Cu and Zn on supported MgO/SiO_2 catalysts during ethanol conversion to 1,3-Butadiene, ACS Catal 9 (2019) 269–285, doi:10.1021/acscatal.8b03515.
[9] S. Li, Y. Men, J. Wang, S. Liu, X. Wang, F. Ji, S. Chai, Q. Song, Morphological control of inverted MgO-SiO_2 composite catalysts for efficient conversion of ethanol to 1,3-butadiene, Appl. Catal. A Gen. 577 (2019) 1–9, doi:10.1016/j.apcata.2019.03.007.
[10] H.T. Abdulrazzaq, A. Rahmani Chokanlu, B.G. Frederick, T.J. Schwartz, Reaction kinetics analysis of ethanol dehydrogenation catalyzed by MgO–SiO_2, ACS Catal 10 (2020) 6318–6331, doi:10.1021/acscatal.0c00811.
[11] X. Wang, Y. Men, J. Wang, S. Liu, Q. Song, M. Yang, The influence of zinc loadings on the selectivity control of bio-ethanol transformation over MgO-SiO_2 catalysts, Appl. Catal. A Gen. 598 (2020) 117565, doi:10.1016/j.apcata.2020.117565.
[12] B. Szabó, G. Novodárszki, Z. Pászti, A. Domján, J. Valyon, J. Hancsók, R. Barthos, MgO−SiO_2 Catalysts for the ethanol to butadiene reaction: the effect of Lewis acid promoters, ChemCatChem 12 (2020) 5686–5696, doi:10.1002/cctc.202001007.
[13] B. Szabó, G. Novodárszki, Z. May, J. Valyon, J. Hancsók, R. Barthos, Conversion of ethanol to butadiene over mesoporous In_2O_3-promoted MgO-SiO_2 catalysts, Mol. Catal. 491 (2020) 110984, doi:10.1016/j.mcat.2020.110984.
[14] W. Reschetilowski, M. Hauser, F. Alscher, M. Klauck, G. Kalies, Studies on the binary MgO/SiO_2 mixed oxide catalysts for the conversion of ethanol to 1,3-butadiene, Catalysts 10 (2020) 1–17, doi:10.3390/catal10080854.
[15] P.I. Kyriienko, O.V. Larina, D.Y. Balakin, A.O. Stetsuk, Y.M. Nychiporuk, S.O. Soloviev, S.M. Orlyk, 1,3-Butadiene production from aqueous ethanol over ZnO/MgO-SiO_2 catalysts: insight into H_2O effect on catalytic performance, Appl. Catal. A Gen. 616 (2021) 118081, doi:10.1016/j.apcata.2021.118081.
[16] S.H. Chung, A. Ramirez, T. Shoinkhorova, I. Mukhambetov, E. Abou-Hamad, S. Telalovic, J. Gascon, J. Ruiz-Martínez, The importance of thermal treatment on wet-kneaded silica–magnesia catalyst and Lebedev ethanol-to-butadiene process, Nanomaterials 11 (2021) 1–17, doi:10.3390/nano11030579.
[17] S. Shylesh, A.A. Gokhale, C.D. Scown, D. Kim, C.R. Ho, A.T. Bell, From sugars to wheels: the conversion of ethanol to 1,3-butadiene over metal-promoted magnesia-silicate catalysts, ChemSusChem 9 (2016) 1462–1472, doi:10.1002/cssc.201600195.
[18] C. Angelici, M.E.Z. Velthoen, B.M. Weckhuysen, P.C.A. Bruijnincx, Effect of preparation method and CuO promotion in the conversion of ethanol into 1,3-butadiene over SiO_2–MgO catalysts, ChemSusChem 7 (2014) 2505–2515, doi:10.1002/cssc.201402361.
[19] M. Zhang, M. Gao, J. Chen, Y. Yu, Study on key step of 1,3-butadiene formation from ethanol on MgO/SiO_2, RSC Adv 5 (2015) 25959–25966, doi:10.1039/C4RA17070A.
[20] C. Angelici, F. Meirer, A.M.J. Van Der Eerden, H.L. Schaink, A. Goryachev, J.P. Hofmann, E.J.M. Hensen, B.M. Weckhuysen, P.C.A. Bruijnincx, Ex situ and operando studies on the role of copper in Cu-promoted SiO_2-MgO catalysts for the Lebedev ethanol-to-butadiene process, ACS Catal 5 (2015) 6005–6015, doi:10.1021/acscatal.5b00755.
[21] C. Angelici, M.E.Z. Velthoen, B.M. Weckhuysen, P.C.A. Bruijnincx, Influence of acid-base properties on the Lebedev ethanol-to-butadiene process catalyzed by SiO_2-MgO materials, Catal. Sci. Technol. 5 (2015) 2869–2879, doi:10.1039/c5cy00200a.
[22] S.H. Chung, C. Angelici, S.O.M. Hinterding, M. Weingarth, M. Baldus, K. Houben, B.M. Weckhuysen, P.C.A. Bruijnincx, Role of magnesium silicates in wet-kneaded silica-magnesia catalysts for the Lebedev ethanol-to-butadiene process, ACS Catal 6 (2016) 4034–4045, doi:10.1021/acscatal.5b02972.
[23] W.E. Taifan, G.X. Yan, J. Baltrusaitis, Surface chemistry of MgO/SiO_2 catalyst during the ethanol catalytic conversion to 1,3-butadiene: in-situ DRIFTS and DFT study, Catal. Sci. Technol. 7 (2017) 4648–4668, doi:10.1039/c7cy01556a.
[24] X. Huang, Y. Men, J. Wang, W. An, Y. Wang, Highly active and selective binary MgO-SiO_2 catalysts for the production of 1,3-butadiene from ethanol, Catal. Sci. Technol. 7 (2017) 168–180, doi:10.1039/c6cy02091g.
[25] W.E. Taifan, J. Baltrusaitis, In situ spectroscopic insights on the molecular structure of the MgO/SiO_2 catalytic active sites during ethanol conversion to 1,3-butadiene, J. Phys. Chem. C. 122 (2018) 20894–20906, doi:10.1021/acs.jpcc.8b06767.
[26] O.V. Larina, P.I. Kyriienko, D.Y. Balakin, M. Vorokhta, I. Khalakhan, Y.M. Nychiporuk, V. Matolín, S.O. Soloviev, S.M. Orlyk, Effect of ZnO on acid-base properties and catalytic performances of ZnO/ZrO_2-SiO_2 catalysts in 1,3-butadiene production from ethanol-water mixture, Catal. Sci. Technol. 9 (2019) 3964–3978, doi:10.1039/c9cy00991d.
[27] O.V. Larina, N.D. Shcherban, P.I. Kyriienko, I.M. Remezovskyi, P.S. Yaremov, I. Khalakhan, G. Mali, S.O. Soloviev, S.M. Orlyk, S. Dzwigaj, Design of effective catalysts based on ZnLaZrSi oxide systems for obtaining 1,3-butadiene from aqueous ethanol, ACS Sustain. Chem. Eng. 8 (2020) 16600–16611, doi:10.1021/acssuschemeng.0c05925.
[28] G. Pomalaza, P. Simon, A. Addad, M. Capron, F. Dumeignil, Properties and activity of Zn-Ta-TUD-1 in the Lebedev process, Green Chem 22 (2020) 2558–2574, doi:10.1039/d0gc00103a.
[29] G. Pomalaza, M. Capron, F. Dumeignil, Improving the synthesis of Zn-Ta-TUD-1 for the Lebedev process using the design of experiments methodology, Appl. Catal. A Gen. 591 (2020) 117386, doi:10.1016/j.apcata.2019.117386.
[30] L. Qi, Y. Zhang, M.A. Conrad, C.K. Russell, J. Miller, A.T. Bell, Ethanol conversion to butadiene over isolated zinc and yttrium sites grafted onto dealuminated beta zeolite, J. Am. Chem. Soc. 142 (2020) 14674–14687, doi:10.1021/jacs.0c06906.
[31] A. Miyaji, M. Hiza, Y. Sekiguchi, S. Akiyama, A. Shiga, T. Baba, Catalysis by MgO and the role of Zn^{2+} in talc catalysts for the selective production of 1,3-butadiene from ethanol, J. Japan Pet. Inst. 61 (2018) 171–181, doi:10.1627/jpi.61.171.
[32] W.C. Li, A.H. Lu, C. Weidenthaler, F. Schüth, Hard-templating pathway to create mesoporous magnesium oxide, Chem. Mater. 16 (2004) 5676–5681, doi:10.1021/cm048759n.
[33] S. Jarczewski, M. Drozdek, P. Michorczyk, C. Cuadrado-Collados, J. Gandara-Loe, J. Silvestre-Albero, L. Lityńska-Dobrzyńska, P. Kuśtrowski, On the catalytic role of superficial VOx species and coke deposited on mesoporous MgO replica in oxidative dehydrogenation of ethylbenzene, Appl. Surf. Sci. 504 (2020) 144336, doi:10.1016/j.apsusc.2019.144336.
[34] H. Tamon, H. Ishizaka, Influence of gelation temperature and catalysts on the mesoporous structure of resorcinol-formaldehyde aerogels, J. Colloid Interface Sci. 223 (2000) 305–307, doi:10.1006/jcis.1999.6640.

[35] M. Yoshimune, T. Yamamoto, M. Nakaiwa, K. Haraya, Preparation of highly mesoporous carbon membranes via a sol-gel process using resorcinol and formaldehyde, Carbon N. Y. 46 (2008) 1031–1036, doi:10.1016/j.carbon.2008.03.007.
[36] K.Z. Gaca, J. Sefcik, Mechanism and kinetics of nanostructure evolution during early stages of resorcinol-formaldehyde polymerisation, J. Colloid Interface Sci. 406 (2013) 51–59, doi:10.1016/j.jcis.2013.05.062.
[37] M. Mohai, X.P.S. MultiQuant, multimodel XPS quantification software, Surf. Interface Anal 36 (2004) 828–832, doi:10.1002/sia.1775.
[38] S. Evans, R.G. Pritchard, J.M. Thomas, Relative differential subshell photoionisation cross-sections (MgKα) from lithium to uranium, J. Electron Spectros. Relat. Phenomena. 14 (1978) 341–358, doi:10.1016/0368-2048(78)80008-5.
[39] R.F. Reilman, A. Msezane, S.T. Manson, Relative intensities in photoelectron spectroscopy of atoms and molecules, J. Electron Spectros. Relat. Phenomena. 8 (1976) 389–394, doi:10.1016/0368-2048(76)80025-4.
[40] M. Mohai, I. BertótiH.J. Mathieu, B. Reihl, D. Briggs (Eds.), Correction for surface contaminations in XPS: a practical approach, ECASIA 95 (1996) 675–678.